THE GEOLOGICAL SOCIETY OF AMERICA®

Elastic geothermobarometry: Corrections for the geometry of the host-inclusion system

M.L. Mazzucchelli[1]*, P. Burnley[2], R.J. Angel[1], S. Morganti[3], M.C. Domeneghetti[1], F. Nestola[4], and M. Alvaro[1]
[1]Department of Earth and Environmental Sciences, University of Pavia, 27100 Pavia, Italy
[2]Department of Geosciences and High Pressure Science and Engineering Center, University of Nevada, Las Vegas, Nevada 89154, USA
[3]Department of Electrical, Computer, and Biomedical Engineering, University of Pavia, 27100 Pavia, Italy
[4]Department of Geosciences, University of Padua, 35131 Padua, Italy

ABSTRACT

Elastic geothermobarometry on inclusions is a method to determine pressure-temperature conditions of mineral growth independent of chemical equilibrium. Because of the difference in their elastic properties, an inclusion completely entrapped inside a host mineral will develop a residual stress upon exhumation, from which one can back-calculate the entrapment pressure. Current elastic geobarometric models assume that both host and inclusion are elastically isotropic and have an ideal geometry (the inclusion is spherical and isolated at the center of an infinite host). These conditions do not commonly occur in natural rocks, and the consequences for inclusion pressures can only be quantified with numerical approaches. In this paper, we report the results of numerical simulations of inclusions with the finite element method on elastically isotropic systems. We define and determine a geometrical factor (Γ) that allows measured residual pressures to be corrected for the effects of non-ideal geometry. We provide simple guidelines as to which geometries can safely be used for elastic geobarometry without correcting for the geometry. We also show that the discrepancies between elastic and conventional geobarometry reported in literature are not due to geometrical effects, and therefore result from other factors not yet included in current models.

INTRODUCTION

Application of conventional geothermobarometry is extremely challenging in many rock types due to alteration processes, chemical reequilibration and diffusion, and kinetic limitations. Elastic geothermobarometry on host-inclusion systems is a complementary method independent of chemical equilibrium. An inclusion completely entrapped inside a host mineral will develop a residual stress upon exhumation because of the contrast in elastic properties (Rosenfeld and Chase, 1961). If the host does not undergo plastic deformation or brittle failure after trapping the inclusion, the entrapment pressure (P_{trap}) can be calculated from the measured residual pressure on the inclusion (or remnant pressure, P_{inc}), provided that the elastic properties (equations of state, EoS) for the host and inclusion are known (e.g., Zhang, 1998; Angel et al., 2014). Elastic geothermobarometry is increasingly applied to metamorphic rocks, where measurements of Raman shifts on quartz inclusions trapped in garnet (quartz-in-garnet inclusion barometry, QuiG) give information on the residual stresses that can be used to infer growth conditions (e.g., Kouketsu et al., 2016) and the degree of overstepping of garnet isograds (e.g., Spear et al., 2014).

The validity of elastic geobarometric methods was discussed by Ashley et al. (2016), who reported that the P_{trap} inferred from measured P_{inc} of quartz inclusions in garnets do not match those obtained by conventional geobarometry on the same rocks. However, the calculation of P_{trap} currently assumes that the minerals are elastically isotropic with ideal geometry where the inclusion is spherical and isolated at the center of the host (Goodier, 1933; Eshelby, 1957; Van der Molen and Van Roermund, 1986). None of these conditions apply in natural systems; neither quartz nor garnet are elastically isotropic, inclusions are often close to grain boundaries or other inclusions, and they are often not spherical. The resulting changes in P_{inc} can only be quantified using numerical approaches.

In this paper, we use finite element (FE) models of elastically isotropic host-inclusion systems with non-ideal geometries to determine the magnitude of the geometric effects on P_{inc}, and in turn on the calculated P_{trap}. We show that the discrepancies reported by Ashley et al. (2016) are only partly due to the geometry of their samples. We provide guidelines as to which geometries of host-inclusion systems lead to deviations smaller than the typical experimental uncertainties in inclusion pressures obtained from conventional μ-Raman measurements, and can therefore be safely used for geobarometry without any correction.

METHODS

The final stress state of an inclusion is path independent, and it is convenient to split the pressure-temperature (*P*-*T*) change from the entrapment conditions (P_{trap}, T_{trap}; see Fig. 1) to the final pressure and temperature (P_{end}, T_{end}) into two parts (see Angel et al., 2014). Figure 1 illustrates the stepwise procedure used to calculate the residual pressure from known entrapment conditions. During step 1 the temperature is reduced from T_{trap} to T_{end} along the isomeke (Rosenfeld and Chase, 1961; Adams et al., 1975), thus preserving the reciprocal mechanical equilibrium between the host and the inclusion. The change in external *T* and *P* required to maintain the pressure in the inclusion equal to the external *P* can be calculated directly from the thermodynamic properties of the minerals without any influence of the geometry of the system. In step 2, the isothermal decompression from P_{foot}, T_{end} to the final P_{end}, T_{end} (P_{foot} T_{end} and P_{end} as defined by Angel et al. [2014]) causes a mechanical disequilibrium between the host and the inclusion. Consequently, the stresses are readjusted through the relaxation process. Because the relaxation depends on force balance at the interface between host and inclusion, in this step the geometry becomes important. The exact amount of relaxation in step 2 can only be calculated if the geometry of the system is ideal; for all other cases a numerical approach is required.

In our study we used two commercially available engineering packages (MARC Mentat by MSC Software, http://www.mscsoftware.com/product/marc/, and Abaqus by Dassault Systèmes, https://www.3ds.com/products-services/simulia/products/abaqus/) to create and solve two-dimensional (2-D) axisymmetric and 3-D models using FE numerical simulations. Always using isotropic elastic properties, we explored the effects of several deviations from ideal geometry, including the size of the inclusion relative to the host and its proximity to external surfaces. To evaluate the effects of non-spherical shapes we modeled ellipsoids of revolution with

*E-mail: mattialuca.mazzucchelli01@universitadipavia.it

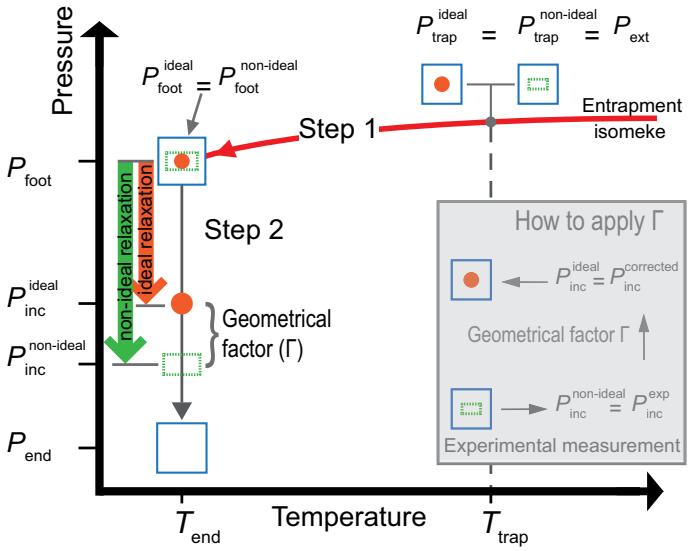

Figure 1. Calculation procedure for two host inclusion pairs; one with ideal geometry (red dot inclusion) and one with non-ideal geometry (green dashed rectangle), that are trapped at the same pressure and temperature (P_{trap}, T_{trap}) conditions. Step 1: Along the isomeke the host and inclusion are in reciprocal mechanical equilibrium. Therefore, the pressure on the isomeke at the final T_{end} (i.e., P_{foot}) will be the same for any geometry of the system. Step 2: The host is decompressed to the final pressure P_{end}. The relaxation of the inclusion is geometry dependent and therefore the final P_{inc} will be different for the two systems ($P^{non-ideal}_{inc} \neq P^{ideal}_{inc}$). The geometrical factor Γ is a measure of this discrepancy. The inset illustrates how to apply Γ to correct the experimental P^{exp}_{inc} measured on natural rocks with non-ideal geometry. The corrected $P^{corrected}_{inc}$ can then be used to back-calculate the P_{trap} using currently available elastic geobarometry models.

aspect ratios 1:1:1, 2:1:1, 1:2:2, 5:1:1, and 1:5:5. The effects of edges and corners were then determined by comparing the results against cylindrical and prismatic models (with quadrilateral cross sections) with the same aspect ratios.

To simulate the effects of external pressure, edge loads (for 2-D models) or face loads (for 3-D models) were applied to the external boundaries of the models. Stationary boundary conditions were placed on the relevant edges and faces to prevent rigid body rotations and translations. An example of a model mesh and the elastic properties used in the models are given in the GSA Data Repository[1]; more details are in Burnley and Davis (2004), Burnley and Schmidt (2006), and Abaqus (2016). For each model, we performed calculations using different elastic isotropic properties for the host and the inclusion to probe possible scaling laws.

For each geometry we calculated the actual inclusion pressure $P^{non-ideal}_{inc}$ by performing FE simulations upon isothermal decompression from P_{foot} to P_{end}. We define a geometrical factor (hereafter Γ) as the normalized deviation of the actual inclusion pressure from that expected for an ideal isolated spherical inclusion, P^{ideal}_{inc}, for the same decompression:

$$\Gamma = \frac{P^{non\text{-}ideal}_{inc}}{P^{ideal}_{inc}} - 1. \quad (1)$$

The value of Γ is obtained using the linear elastic approximation, so it is independent of the magnitude of $P_{foot} - P_{end}$. Because pressures in natural inclusions are typically <1 GPa (e.g., Ashley et al., 2016), this linear approximation is not significant for most inclusions, and the Γ parameter can be used to correct experimentally determined inclusion pressures ($P^{exp}_{inc} = P^{non-ideal}_{inc}$) for geometric effects:

$$P^{corrected}_{inc} = \frac{P^{exp}_{inc}}{1+\Gamma}. \quad (2)$$

This corrected P_{inc} can then be used to calculate the P_{trap} using isotropic elastic geobarometry models (e.g., Angel et al., 2014, 2017b).

RESULTS AND DISCUSSION

Insights from Finite Element Models

Our FE models have been validated against the analytical exact solution by modeling an ideal infinite spherical system. In practice, the host can be considered infinite when the simulation results do not change upon further increase in the size of the host (Fig. 2A). Our FE models then reproduce the analytical solution for the pressure inside a spherical inclusion well within the expected numerical precision (i.e., 0.2%).

The stress in the region of the host close to the inclusion is always deviatoric (e.g., Zhang, 1998). Therefore, when a large inclusion is surrounded by a thin layer of host crystal, the deviatoric stress extends throughout the volume of the thin host layer, causing the outer boundary of the host to deform. The host is thus no longer able to shield the inclusion from the external pressure. Consequently, the P_{inc} will be partially released. For a spherical inclusion at the center of the host, the pressure release is a function of the size and the properties of the inclusion with respect to the host (Fig. 2A). Hosts much stiffer than the inclusion (e.g., quartz in garnet) can preserve a larger P_{inc}. Our results indicate that, if the radius of the host is at least four times that of the inclusion, both the $P^{non-ideal}_{inc}$ and the $P^{non-ideal}_{trap}$ are within 1% of the value expected for an infinite host. For the same reason, the capacity of the host to act as a pressure vessel for the inclusion is also reduced when a small inclusion is close to the external surface of the host (Fig. 2B). Stiffer hosts preserve more residual pressure than softer hosts. Regardless of the contrast in elastic properties, if the inclusion is at least 3 radii from the external surface of the host the effect on P_{inc} is <1%. If a spherical and isotropic inclusion is close to the external surface of the host, the normal stresses in the inclusion are not homogeneous, and the domains of the inclusion closer to the external surface record stresses lower than those toward the center of the host. For a quartz inclusion in pyrope the variation of the pressure across the inclusion can reach 8% when the distance to the surface is half the radius of the inclusion (inset in Fig. 2B). Note that these conclusions do not depend on the absolute size of the inclusion, but upon the relative sizes of the inclusion and host.

For fluid inclusions the aspect ratio and the presence of corners and edges are two major influences on the pressures of isolated inclusions (e.g., Burnley and Davis, 2004; Burnley and Schmidt, 2006). In our models of solid inclusions, we find that the aspect ratio of the inclusion gives rise to deviations in P_{inc} >7% for soft platy inclusions (aspect ratio 1:5:5) in stiff hosts (e.g., quartz in pyrope; see Fig. 3). The presence of edges and corners further enhances the deviations (≈9%). For non-spherical shapes with edges and corners, the stress in the inclusion is neither homogeneous nor hydrostatic. The pressure varies from the center of the inclusion toward its external surface, by different amounts in different directions. For a quartz inclusion with aspect ratio 1:5:5 in pyrope, the pressure variation along the longer axes of the inclusion is ~5%, while it is <1% along the shortest axis (see Figs. DR2 and DR3 in the Data Repository). For a residual pressure at the center of the inclusion of 0.3 GPa, the differential stress ($\sigma_{max} - \sigma_{min}$) within the inclusion reaches 0.28 GPa. For a stiff inclusion in a soft host with the same shape, the pressure variation within the inclusion is typically much larger (e.g., 22% for diamond in pyrope) and of the opposite sign (see Fig. DR2).

The exact effect of inclusion shape on $P^{non-ideal}_{inc}$ is a complex interplay between the bulk and shear moduli for both host and inclusion (see Fig. 3).

[1]GSA Data Repository item 2018057, elastic geothermobarometry (computational details, elastic properties used for all calculations, and some additional examples), is available online at http://www.geosociety.org/datarepository/2018/ or on request from editing@geosociety.org.

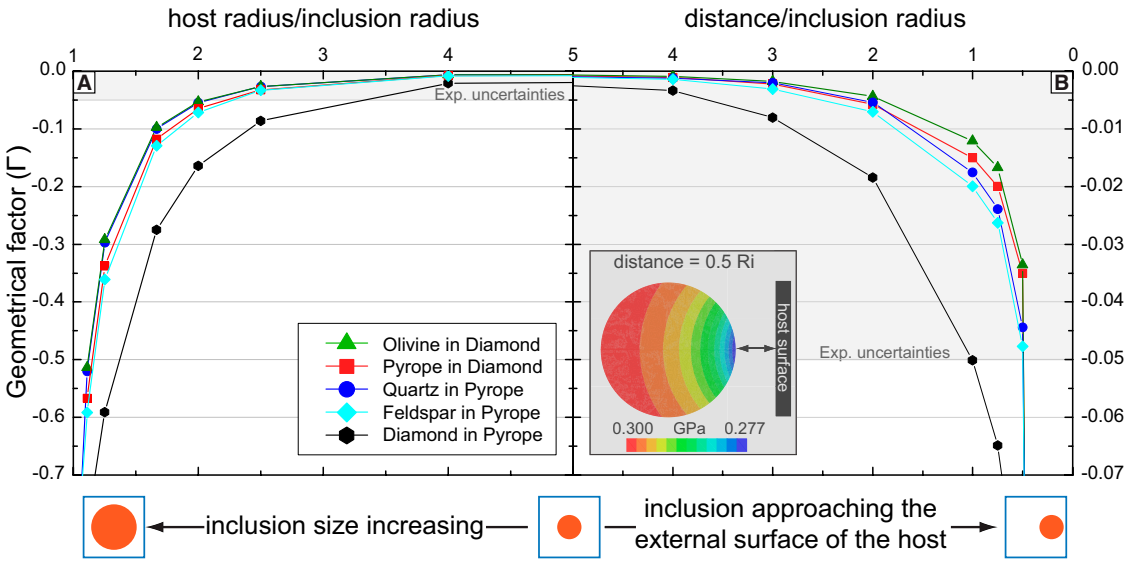

Figure 2. Effects of inclusion size and proximity to the external surface. A: Geometrical factor Γ for a spherical inclusion with increasing size (toward the left) with respect to that of the host. Exp.—experimental. B: Geometrical factor Γ for a spherical inclusion approaching the external surface of the host (toward the right). Γ is always negative when the distance of the inclusion from the external surface is reduced or when the size of the inclusion increases. This can be interpreted as the pressure in the inclusion (P_{inc}) being reduced from the ideal P_{inc}. Inset: Stress map of a model of a quartz inclusion in pyrope, where the distance between the inclusion and the external surface of the host was one-half of the inclusion radius (Ri), showing the inhomogeneity of the pressure.

In general, the influence of non-ideal shapes becomes greater when the bulk modulus of the host and the inclusion are similar, provided there is a significant contrast in shear moduli. For a soft inclusion in a stiffer host (quartz in garnet, or pyrope in diamond) with aspect ratios less than 1:2:2, the deviations induced by the shape are typically <5% (Fig. 3).

Calculation of Entrapment Pressures

Ashley et al. (2016) used Raman spectroscopy to determine the remnant pressure in quartz inclusions in garnets while they were heated up to 500 °C. As the T increases, the P_{inc}^{exp} increases because of thermal pressure effects, but the P_{trap} for a single inclusion should always be a unique value independent of the temperature (T_{end}) at which the P_{inc}^{exp} is measured. However, Ashley et al. (2016) reported large variations on P_{trap} for the same inclusion calculated from the various P_{inc}^{exp} measured at different T_{end} and none of the calculated P_{trap} agreed with the results from conventional geobarometry. Ashley et al. (2016) ascribed this unphysical behavior to the use of unrealistic EoS for quartz close to the α-β structural phase transition. We chose this example to assess if the shape of the inclusion could explain these discrepancies.

We consider the case of sample MT 09-09, where several quartz inclusions are entrapped in an almandine-rich garnet (Ashley et al., 2015, 2016). The P_{trap} values at 540 °C were recalculated from the experimental P_{inc}^{exp} of 0.300 GPa and 0.491 GPa at the minimum and maximum T_{end} (31 °C and 500 °C) using a more reliable EoS for quartz (Angel et al., 2017a) that explicitly includes the α-β transition. Assuming ideal geometry for the quartz inclusion, the discrepancy between the two P_{trap} values is 0.186 GPa (Table 1), similar to that reported by Ashley et al. (2016), demonstrating that the differences cannot be ascribed to errors in the EoS. To eliminate the discrepancies in P_{trap} values the volume thermal expansion of almandine must be increased by more than 30% to α_{298K} ~2.76 × 10^{-5} K^{-1}; this is unrealistic given that this value is much greater than those of any silicate garnet end member.

Because the shapes of the inclusions measured by Ashley et al. (2016) were not reported, we then overestimated the shape effects by modeling the inclusion as a platy prism (aspect ratio 1:5:5). At room temperature the correction factor is Γ = −0.094, similar to that for quartz in pyrope (Fig. 3), but decreases to Γ = −0.078 at 500 °C (Table 1) due to the elastic softening of quartz as it approaches the phase transition (Lakshtanov et al., 2007). The inclusion pressures corrected for shape, $P_{inc}^{corrected}$, are then 0.331 GPa (at 31 °C) and 0.532 GPa (at 500 °C), and result in a small but

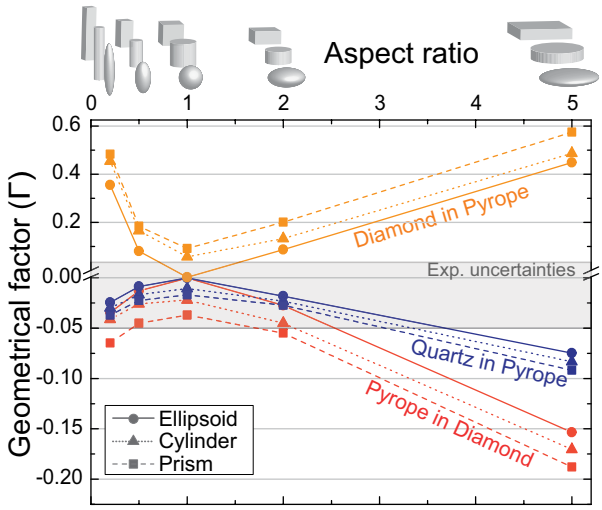

Figure 3. Geometrical factor Γ for several shapes plotted versus the normalized aspect ratio. The latter is calculated with the unique axis as the denominator (e.g., aspect ratio 2:1:1 becomes ½ = 0.5). For a soft inclusion in a stiffer host (e.g., quartz in garnet), Γ < 0 and therefore $P_{inc}^{non\text{-}ideal} < P_{inc}^{ideal}$ (as in Fig. 1). The opposite occurs for a stiff inclusion in a softer host (e.g., diamond in pyrope). Note that Γ values greater than zero are plotted with a compressed vertical scale. Exp.—experimental.

TABLE 1. CALCULATION OF ENTRAPMENT PRESSURE FOR SAMPLE MT 09-09 BEFORE AND AFTER THE CORRECTION FOR THE SHAPE OF THE INCLUSION

Uncorrected for shape			Correction for shape		
T_{end} (°C)	P_{inc}^{exp} (GPa)	P_{trap} at 540 °C from P_{inc}^{exp} (GPa)	Geometrical factor (Γ)	$P_{inc}^{corrected}$ (GPa)	P_{trap} at 540 °C from $P_{inc}^{corrected}$ (GPa)
31	0.300	1.041	−0.094	0.331	1.091
500	0.491	0.855	−0.078	0.532	0.929
		ΔP_{trap}=0.186			ΔP_{trap}=0.162

Note: P_{trap} is entrapment pressure. ΔP_{trap} is calculated as the difference between P_{trap} from the pressure on the inclusion (P_{inc}) at the end temperature T_{end} = 31 °C, and that from the P_{inc} at 500 °C (exp is experimental). The equations of state used for quartz and almandine are reported in the GSA Data Repository (see text footnote 1).

insignificant reduction of 0.02 GPa in the differences in P_{trap} calculated from the two measurements. Furthermore, even with the geometrical correction, the P_{trap} values (1.091 and 0.929 GPa) are not in agreement with those obtained from the conventional methods (0.82 GPa; Ashley et al., 2015).

Thus neither the EoS nor the shape of the inclusion can explain the discrepancies found by Ashley et al. (2016), and other factors not yet included in the current models must be responsible for the discrepancies in the P_{trap}. One factor is that quartz inclusions in a garnet host will be subject to isotropic strain (leaving aside further perturbations arising from the elastic relaxation and the geometry) because garnet is cubic. As quartz is elastically anisotropic, the isotropic strain will result in a non-hydrostatic stress in the inclusion. The effect of this deviatoric stress on the Raman spectrum of quartz is not known in detail, but both theory (Key, 1967) and experiments (Briggs and Ramdas, 1977) show that Raman peak shifts will be different from those predicted from hydrostatic calibrations used by Ashley et al. (2016) to convert measured Raman shifts into pressures. Therefore, the mismatch in the P_{trap} is probably due to the combination of an inappropriate Raman stress calibration and the assumption of elastic isotropy in the geobarometric models.

CONCLUSIONS

Current elastic geobarometric models assume isotropic elastic properties for the host and the inclusion, and that the inclusions are isolated and spherical. These conditions do not commonly occur in natural rocks. Regardless of the relative stiffness of host and inclusion, for a big inclusion in a small host and for an inclusion close to the external surface of the host, the P_{inc}^{exp} is reduced relative to the ideal case, but a simple correction factor cannot be defined and Γ should be evaluated on a case-by-case basis with finite element method (FEM) analysis carried out on realistic digital models of the inclusions.

For isotropic elasticity, our FEM results show that for an inclusion at least at 3 radii from external surfaces or other inclusions, the geometric effects on P_{inc}^{exp} are <1% (Fig. 2B). Under these conditions the shape effects then dominate the geometric corrections to the measured P_{inc}^{exp} (Fig. 3). For soft inclusions in a stiff host (e.g., quartz in garnet), non-spherical inclusions ($\Gamma < 0$), will exhibit a lower pressure than spherical inclusions. Correction of the measured P_{inc}^{exp} for the shape effects will therefore result in $P_{inc}^{corrected} > P_{inc}^{exp}$ and thus an increase in the calculated P_{trap}. By contrast, for stiff inclusions in soft hosts ($\Gamma > 0$), the correction will lead to $P_{inc}^{corrected} < P_{inc}^{exp}$ and therefore a reduction in P_{trap}. Experimental uncertainties on P_{inc}^{exp} are typically <5% when measured by Raman spectroscopy (e.g., Ashley et al., 2016, Kouketsu et al., 2016). For P_{inc} <1 GPa, the uncertainties propagated into the P_{trap} are smaller than those on the P_{inc}. Therefore, pressures from inclusions for which the geometrical effects on P_{inc}^{exp} are <5% will provide reliable estimates of P_{inc}, and hence P_{trap} without the need for correction. For soft inclusions in stiff hosts, such as quartz in garnet, this means the following:

(1) The radius of the inclusion must be smaller than one-half of that of the host.

(2) The distance from the external surface is larger than one-half the radius of the inclusion.

(3) The inclusion aspect ratio is lower than 1:3:3, with few sharp edges and corners.

These guidelines do not apply to inclusions stiffer than the host (e.g., diamond in garnet) that require much larger corrections of opposite sign (Fig. 3).

ACKNOWLEDGMENTS

This project received funding from the European Research Council under the European Union's Horizon 2020 research and innovation program grant agreements 714936 to Alvaro and 307322 to Nestola. Alvaro has also been supported by the MIUR-SIR (Ministry of Education, University and Research–Scientific Independence of Young Researchers, Italy) grant MILE DEEp (Mineral Inclusion Elasticity for a New Deep Subduction Geobarometer; RBSI140351). Support for P. Burnley and computational resources was provided by the U.S. National Nuclear Security Administration under the Stewardship Science Academic Alliances program through U.S. Department of Energy Cooperative Agreement DE-NA0001982. We thank Matthew Steele-MacInnis and two anonymous reviewers for very constructive comments on the manuscript.

REFERENCES CITED

Abaqus, 2016, Abaqus Documentation: Providence, Rhode Island, Dassault Systèmes, http://50.16.225.63/v2016/.

Adams, H.G., Cohen, L.H., and Rosenfeld, J.L., 1975, Solid inclusion piezothermometry I: Comparison dilatometry: American Mineralogist, v. 60, p. 574–583.

Angel, R.J., Mazzucchelli, M.L., Alvaro, M., Nimis, P., and Nestola, F., 2014, Geobarometry from host-inclusion systems: The role of elastic relaxation: American Mineralogist, v. 99, p. 2146–2149, https://doi.org/10.2138/am-2014-5047.

Angel, R.J., Alvaro, M., Miletich, R., and Nestola, F., 2017a, A simple and generalised P-T-V EoS for continuous phase transitions, implemented in EosFit and applied to quartz: Contributions to Mineralogy and Petrology, v. 172, p. 29, https://doi.org/10.1007/s00410-017-1349-x.

Angel, R.J., Mazzucchelli, M.L., Alvaro, M., and Nestola, F., 2017b, EosFit-Pinc: A simple GUI for host-inclusion elastic thermobarometry: American Mineralogist, v. 102, p. 1957–1960, https://doi.org/10.2138/am-2017-6190.

Ashley, K.T., Thigpen, J.R., and Law, R.D., 2015, Prograde evolution of the Scottish Caledonides and tectonic implications: Lithos, v. 224–225, p. 160–178, https://doi.org/10.1016/j.lithos.2015.03.011.

Ashley, K.T., Steele-MacInnis, M., Bodnar, R.J., and Darling, R.S., 2016, Quartz-in-garnet inclusion barometry under fire: Reducing uncertainty from model estimates: Geology, v. 44, p. 699–702, https://doi.org/10.1130/G38211.1.

Briggs, R.J., and Ramdas, A.K., 1977, Piezospectroscopy of the Raman spectrum of α-quartz: Physical Review B: Condensed Matter and Materials Physics, v. 16, p. 3815–3826, https://doi.org/10.1103/PhysRevB.16.3815.

Burnley, P.C., and Davis, M.K., 2004, Volume changes in fluid inclusions produced by heating and pressurization: An assessment by finite element modeling: Canadian Mineralogist, v. 42, p. 1369–1382, https://doi.org/10.2113/gscanmin.42.5.1369.

Burnley, P.C., and Schmidt, C., 2006, Finite element modeling of elastic volume changes in fluid inclusions: Comparison with experiment: American Mineralogist, v. 91, p. 1807–1814, https://doi.org/10.2138/am.2006.2036.

Eshelby, J.D., 1957, The determination of the elastic field of an ellipsoidal inclusion, and related problems: Royal Society of London Proceedings, ser. A, v. 241, p. 376–396, https://doi.org/10.1098/rspa.1957.0133.

Goodier, J.N., 1933, Concentration of stress around spherical and cylindrical inclusions and flaws: Journal of Applied Mechanics, v. 55, p. 39–44.

Key, S.W., 1967, Grüneisen tensor for anisotropic materials: Journal of Applied Physics, v. 38, p. 2923–2928, https://doi.org/10.1063/1.1710025.

Kouketsu, Y., Hattori, K., Guillot, S., and Rayner, N., 2016, Eocene to Oligocene retrogression and recrystallization of the Stak eclogite in northwest Himalaya: Lithos, v. 240–243, p. 155–166, https://doi.org/10.1016/j.lithos.2015.10.022.

Lakshtanov, D.L., Sinogeikin, S.V., and Bass, J.D., 2007, High-temperature phase transitions and elasticity of silica polymorphs: Physics and Chemistry of Minerals, v. 34, p. 11–22, https://doi.org/10.1007/s00269-006-0113-y.

Rosenfeld, J.L., and Chase, A.B., 1961, Pressure and temperature of crystallization from elastic effects around solid inclusions in minerals?: American Journal of Science, v. 259, p. 519–541, https://doi.org/10.2475/ajs.259.7.519.

Spear, F.S., Thomas, J.B., and Hallet, B.W., 2014, Overstepping the garnet isograd: A comparison of QuiG barometry and thermodynamic modeling: Contributions to Mineralogy and Petrology, v. 168, p. 1059, https://doi.org/10.1007/s00410-014-1059-6.

Van der Molen, I., and Van Roermund, H.L.M., 1986, The pressure path of solid inclusions in minerals: The retention of coesite inclusions during uplift: Lithos, v. 19, p. 317–324, https://doi.org/10.1016/0024-4937(86)90030-7.

Zhang, Y., 1998, Mechanical and phase equilibria in inclusion-host systems: Earth and Planetary Science Letters, v. 157, p. 209–222, https://doi.org/10.1016/S0012-821X(98)00036-3.

Manuscript received 13 October 2017
Revised manuscript received 3 December 2017
Manuscript accepted 4 December 2017

Printed in USA